INTERNATIONAL JOURNAL FOR NUMERICAL METHODS IN FLUIDS, VOL. 14, 477–493 (1992)

A STABLE ALGORITHM FOR BED FRICTION IN THREE-DIMENSIONAL SHALLOW SEA MODAL MODELS

A. M. DAVIES

Proudman Oceanographic Laboratory, Bidston Observatory, Birkenhead, Merseyside L43 7RA, U.K.

AND

J. N. ALDRIDGE

MAFF Fisheries Laboratory, Pakefield Road, Lowestoft, Suffolk NR33 OHT, U.K.

SUMMARY

The mathematical formulation of a three-dimensional shallow sea model using a modal expansion in the vertical is briefly described.

The importance of the time discretization of the vertical diffusion term and bottom friction term is discussed in some detail. Both stability theory and numerical calculations show the importance of time centring or evaluating the modal form of the viscosity term at the higher time step in order to develop a numerically efficient algorithm. Similar analysis and calculations show that in shallow water it is essential to time centre or evaluate bottom friction at the higher time step. In the case of linear bottom friction it is shown that this condition can be readily accomplished. However, using a quadratic friction formulation (a more physically realistic form), this cannot be readily achieved. A new algorithm is presented whereby a stable solution can be obtained even in shallow water using quadratic bottom friction.

KEY WORDS Bed friction Hydrodynamics Shallow sea Galerkin

1. INTRODUCTION

With increasing interest in near-coastal problems, in particular the movement of sediment (both as bed load and suspended load) under the action of waves and current,[1] there is an increasing demand to develop three-dimensional models which can yield accurate bed stresses and current profiles in shallow water regions.

Three-dimensional models using a finite difference representation in the vertical are one way of approaching the problem and a range of numerical methods (e.g. Crank–Nicholson, Dufort–Frankel, Saul'ev)[2–4] exists for centring the vertical diffusion term in time and ensuring on a regular grid an unconditionally stable method of solving this term. A range of transformation methods (e.g. kappa grid, log or log–linear compressions near the sea bed) aimed at improving the near-bed resolution can be found in Reference 5. Applications using a fixed grid (i.e. a grid on z-co-ordinates) are given by Leendertse *et al.*[6] and a good recent general review of numerical modelling methods is given in Reference 7.

Alternatives to using a finite difference grid in the vertical are to use piecewise functions (a finite element approach)[8–10] or continuous functions (a spectral approach).[11–15] The computational

Received January 1991
Revised June 1991

advantages in terms of computer time and increased accuracy of spectral methods compared with a finite difference approach have been demonstrated by Davies and Stephens.[16] Also, the spectral method is ideally suited for the new generation of multiprocessor vector computers.[17,18]

In this paper we consider two simple mathematical models. First, the closed rectangular North Sea basin used by Heaps[11] in his original research concerned with developing three-dimensional models and subsequently used by a number of authors[2,16,19-23] as a 'benchmark' for various numerical methods is considered. Secondly, a simple point model driven by an oscillatory pressure gradient of tidal period is used to examine in more detail the stability of the numerical solution developed here. By this means the method is compared with a standard 'benchmark' solution of wind-driven flow in a sea region and pressure-driven flow of tidal period.

2. MATHEMATICAL MODELS

2.1. *Three-dimensional equations*

The three-dimensional hydrodynamic equations solved by Heaps[11] for wind-induced motion, written in sigma co-ordinates $\sigma = z/h$, are given by

$$\frac{\partial \zeta}{\partial t} + \frac{\partial}{\partial x}\left(h\int_0^1 u\,\mathrm{d}\sigma\right) + \frac{\partial}{\partial y}\left(h\int_0^1 v\,\mathrm{d}\sigma\right) = 0, \tag{1}$$

$$\frac{\partial u}{\partial t} - \gamma v = -g\frac{\partial \zeta}{\partial x} + \frac{1}{h^2}\frac{\partial}{\partial \sigma}\left(\mu\frac{\partial u}{\partial \sigma}\right), \tag{2}$$

$$\frac{\partial v}{\partial t} + \gamma u = -g\frac{\partial \zeta}{\partial y} + \frac{1}{h^2}\frac{\partial}{\partial \sigma}\left(\mu\frac{\partial v}{\partial \sigma}\right), \tag{3}$$

where t is time, x, y and z are Cartesian co-ordinates and u and v are the x- and y-components of velocity. The acceleration due to gravity, g, and the geostrophic coefficient γ are taken as constant, with μ the vertical eddy viscosity, h the water depth and ζ the sea surface elevation above its undisturbed value.

The surface and bed boundary conditions in σ-co-ordinates are given by

$$-\rho\left(\frac{\mu}{h}\frac{\partial u}{\partial \sigma}\right)_0 = F_S, \qquad -\rho\left(\frac{\mu}{h}\frac{\partial v}{\partial \sigma}\right)_0 = G_S, \tag{4}$$

$$-\rho\left(\frac{\mu}{h}\frac{\partial u}{\partial \sigma}\right)_1 = F_B, \qquad -\rho\left(\frac{\mu}{h}\frac{\partial v}{\partial \sigma}\right)_1 = G_B, \tag{5}$$

with ρ the density of sea water.

2.2. *Point model in the vertical*

For a single-point model in the vertical the linear hydrodynamic equations are

$$\frac{\partial u}{\partial t} - \gamma v = \frac{\partial P}{\partial x} + \frac{1}{h^2}\frac{\partial}{\partial \sigma}\left(\mu\frac{\partial u}{\partial \sigma}\right), \tag{6}$$

$$\frac{\partial v}{\partial t} + \gamma u = \frac{\partial P}{\partial y} + \frac{1}{h^2}\frac{\partial}{\partial \sigma}\left(\mu\frac{\partial v}{\partial \sigma}\right). \tag{7}$$

In the model considered later, forced by oscillatory pressure gradients we express $\partial P/\partial x$ and $\partial P/\partial y$ as

$$\frac{\partial P}{\partial x} = h_x \omega \cos(\omega t), \tag{8}$$

$$\frac{\partial P}{\partial y} = h_y \omega \cos(\omega t), \tag{9}$$

with h_x and h_y the amplitude of the oscillatory forcing of frequency ω.

2.3. *Boundary conditions*

At the sea bed a slip condition is applied given by

$$F_B = k\rho U_h Q, \qquad G_B = k\rho V_h Q, \tag{10}$$

with k the coefficient of bottom friction. For linear slip

$$Q = 1, \tag{11}$$

while for quadratic slip

$$Q = (U_h^2 + V_h^2)^{1/2}. \tag{12}$$

At the surface, for wind-induced flows F_S and G_S are the externally applied wind stresses, while for tidal motion they are zero.

In the case of the closed rectangular basin a no-flow condition normal to the edges of the basin is applied.

2.4. *Numerical solution*

Here we briefly outline the major steps in solving the hydrodynamic equations using the Galerkin method in the vertical. In particular, emphasis is placed upon the time discretization of the viscosity terms and bottom frictional terms. For clarity in the point model we consider equation (6) without rotation. Details of the application of the Galerkin method to the solution of the full three-dimensional equations have been given elsewhere[19, 20] and will not be repeated here.

Considering a single-point model in the vertical, the Galerkin method proceeds by expanding the velocity u as time-dependent coefficients $A_r(t)$ and basis functions $f_r(\sigma)$ in the vertical:

$$u = \sum_{r=1}^{m} A_r(t) f_r(\sigma). \tag{13}$$

Applying the Galerkin method to the solution of equation (6) without rotation, the equation is multiplied by each basis function f_k and the term involving the eddy viscosity is integrated by parts. Thus, neglecting rotation, from (6) we obtain

$$\sum_{r=1}^{m} \frac{dA_r}{dt} \int_0^1 f_r f_k \, d\sigma = \frac{\partial P}{\partial x} \int_0^1 f_k \, d\sigma - \frac{\alpha}{h^2} \sum_{r=1}^{m} A_r \int_0^1 \Phi \frac{df_r}{d\sigma} \frac{df_k}{d\sigma} d\sigma + \frac{\mu}{h^2} \frac{\partial u}{\partial \sigma}\bigg|_1 f_k(1) - \frac{\mu}{h^2} \frac{\partial u}{\partial \sigma}\bigg|_0 f_k(0), \tag{14}$$

where $k = 1, 2, \ldots, m$. In deriving (14), we have expressed the eddy viscosity as

$$\mu = \alpha(t)\Phi(\sigma). \tag{15}$$

2.5. Eigenfunction basis set

The choice of basis functions in (14) is arbitrary, but here we will consider eigenfunctions (modes) of an eigenfunction problem involving the vertical eddy viscosity profile. Thus

$$\frac{\mathrm{d}}{\mathrm{d}\sigma}\left(\Phi\frac{\mathrm{d}f}{\mathrm{d}\sigma}\right) = -\varepsilon f, \tag{16}$$

with ε the eigenvalues.

An appropriate surface boundary condition for (16) is a natural boundary condition:

$$\left.\frac{\mathrm{d}f_r}{\mathrm{d}\sigma}\right|_0 = 0. \tag{17}$$

At the sea bed a similar natural boundary condition can be applied:

$$\left.\frac{\mathrm{d}f_r}{\mathrm{d}\sigma}\right|_1 = 0. \tag{18}$$

An alternative is to satisfy the bottom boundary condition (10) exactly. This can be accomplished using (5) and (10). Thus substituting (5) into (10) gives

$$\left.-\frac{\mu}{h}\frac{\partial u}{\partial\sigma}\right|_1 = kQU_h. \tag{19}$$

In order to satisfy (19) for arbitrary coefficients A_r in expansion (13), it is necessary to solve the eigenvalue problem (16) subject to the boundary condition

$$\left.\frac{\mathrm{d}f_r}{\mathrm{d}\sigma}\right|_1 = -\frac{kQh}{\mu}f_r(1). \tag{20}$$

In a full three-dimensional model in which the magnitude of the bottom current Q varies with horizontal position and time, as can the eddy viscosity μ, it would be necessary to solve the eigenvalue problem for each time step and grid point. This is clearly computationally impractical and for this reason the natural boundary condition (18) is preferable, although, as we will show, this can cause some numerical problems.

Boundary condition (20) was used extensively by Heaps[11] for the case of linear bottom friction (i.e. $Q = 1$) and a flat-bottomed region. Here we consider the development of the solution of the Galerkin form of the hydrodynamic equations using both boundary conditions (18) and (20) in order to illustrate the computational stability of the two methods.

To be consistent with Heaps,[11] it is convenient to express the coefficients A_r as

$$A_r = U_r\phi_r, \tag{21}$$

with

$$\phi_r = 1\Big/\int_0^1 f_r^2\,\mathrm{d}\sigma. \tag{22}$$

Thus, using a basis set of eigenfunctions satisfying the natural boundary condition (18) and using the orthogonality property of eigenfunctions, namely

$$\int_0^1 f_r f_k\,\mathrm{d}\sigma \begin{cases} = 0, & r \neq k, \\ \neq 0, & r = k, \end{cases} \tag{23}$$

with

$$a_r = \int_0^1 f_r \, d\sigma, \tag{24}$$

equation (14) gives

natural boundary condition

$$\frac{dU_r}{dt} = \frac{\partial P}{\partial x} a_r + \frac{F_S}{\rho h} f_r(0) - \frac{F_B}{\rho h} f_r(1) - \frac{\alpha \varepsilon_r}{h^2} U_r. \tag{25}$$

The nature of the modes (Figure 1(a)) in the case of the bottom boundary condition (18) is that

$$a_r = 0, \quad r = 2, 3, \ldots, m, \qquad \varepsilon_r = 0, \quad r = 1. \tag{26}$$

Thus equation (25) can be written as an equation involving the pressure gradient,

$$\frac{dU_1}{dt} = \frac{\partial P}{\partial x} a_1 + \frac{F_S}{\rho h} f_1(0) - \frac{F_B}{\rho h} f_1(1), \tag{27}$$

and a set of equations

$$\frac{dU_r}{dt} = \frac{F_S}{\rho h} f_r(0) - \frac{F_B}{\rho h} f_r(1) - \frac{\alpha \varepsilon_r}{h^2} U_r, \quad r = 2, 3, \ldots, m. \tag{28}$$

In the case in which the bottom boundary condition is satisfied exactly (Figure 1(b)) we obtain

essential boundary condition

$$\frac{dU_r}{dt} = \frac{\partial P}{\partial x} a_r + \frac{F_S}{\rho h} f_r(0) - \frac{\alpha \varepsilon_r}{h^2} U_r, \qquad r = 1, 2, \ldots, m \tag{29}$$

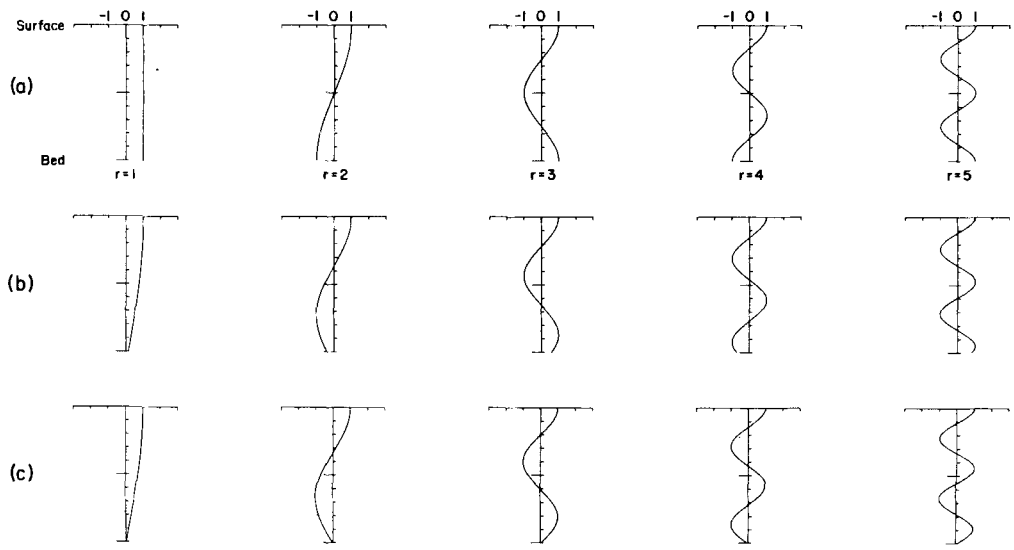

Figure 1. Profiles of the first five modes computed (a) using a zero-derivative boundary condition at the sea bed and satisfying exactly a bottom stress boundary condition, with (b) $k = 0{\cdot}002\,\mathrm{m\,s^{-1}}$, $\mu = 0{\cdot}0130\,\mathrm{m^2\,s^{-1}}$ and (c) $k = 0{\cdot}04\,\mathrm{m\,s^{-1}}$, $\mu = 0{\cdot}0130\,\mathrm{m^2\,s^{-1}}$

It is important to note that the bed stress term does not appear explicitly in equation (29) since in this case the eigenvalue problem has been solved subject to boundary condition (20).

3. TIME DISCRETIZATION AND NUMERICAL STABILITY

In this section we consider various time discretizations of equations (25)–(29) and the associated stability conditions.

3.1. Essential boundary condition

Considering initially equation (29), since terms $\partial P/\partial x$ and $F_S/\rho h$ are externally specified forcing terms, they do not involve U_r; then it is only necessary to consider the equation

$$\frac{dU_r}{dt} = -\frac{\alpha\varepsilon_r}{h^2} U_r \tag{30}$$

in any stability analysis.

A simple two-time-level discretization can be readily accomplished by

$$\frac{U_r^{t+\tau} - U_r^t}{\tau} = -\frac{\alpha\varepsilon_r}{h^2}[\theta U_r^{t+\tau} + (1-\theta) U_r^t], \tag{31}$$

with $\theta = 1{\cdot}0$ giving a fully implicit scheme and $\theta = 0{\cdot}0$ an explicit scheme.

The amplification factor A in the case of the time-differencing scheme (equation (31)) is given by

$$A = \left| \left(1 - \frac{\alpha\varepsilon_r(1-\theta)\tau}{h^2}\right) \Big/ \left(1 + \frac{\alpha\varepsilon_r\theta\tau}{h^2}\right) \right|. \tag{32}$$

In the case of the explicit scheme ($\theta = 0{\cdot}0$) this requires that

$$\tau \leqslant 2h^2/\alpha\varepsilon_r \tag{33}$$

in order to remain stable. For typical values of $h = 5$ m, $\varepsilon_r = 10$ and mean eddy viscosity $\alpha = 0{\cdot}1$ m^2 s^{-1} (see later) this means that τ must be of the order of 25 s, which is clearly impractical. However, since all the modes are uncoupled, the viscosity term can be centred in time or evaluated at the higher time step without requiring any matrix manipulation, giving (equation (32)) an unconditionally stable scheme.

Although an unconditionally stable scheme can be obtained with $\theta = 0{\cdot}5$ (time centring) or $\theta = 1{\cdot}0$ (fully implicit), the amplification factor (equation (32)) for the two schemes is different in shallow water. Thus for illustrative purposes, taking $\varepsilon_r = 10$, $\alpha = 0{\cdot}01$ m^2 s^{-1} and $\tau = 100$ s, for $h = 1$ m we obtain $A = 0{\cdot}667$ when $\theta = 0{\cdot}5$ but $A = 0{\cdot}091$ when $\theta = 1{\cdot}0$. Consequently, in very shallow water ($h = 1$ m) evaluating the viscosity term at the higher time step damps the modes more heavily than time centring the viscosity term. However, in more typical water depths ($h = 10$ m) the amplification factors are not significantly different: $A = 0{\cdot}905$ when $\theta = 0{\cdot}5$ and $A = 0{\cdot}999$ when $\theta = 1{\cdot}0$.

It is clear from this analysis that provided the term involving the eigenvalues ε_r is time centred or evaluated at the higher time step then the solution of the modal equations with the bottom boundary condition satisfied exactly will be unconditionally stable.

3.2. Natural boundary condition

Consider equation (28) in which the bed stress appears as a natural boundary condition. The stability condition for the viscous term is as above, but the analysis for the bed friction term is

more involved. Thus consider the equation

$$\frac{dU_r}{dt} = -\frac{F_B}{\rho h} f_r(1). \tag{34}$$

Substituting for F_B from (10) and for U_h using expansion (13) gives

$$\frac{dU_r}{dt} = -\frac{kQ}{h} f_r(1)\left(U_r \phi_r f_r(1) + \sum_{\substack{i=1 \\ i \neq r}}^{m} U_i \phi_i f_i(1) \right). \tag{35}$$

The complexity in equation (35) is that the bottom friction term couples together all the modes.

If the summation in (35) were not present, then a simple stability condition could be developed as

$$\frac{U_r^{t+\tau} - U_r^t}{\tau} = -\frac{kQ\phi_r f_r^2(1)}{h} [\theta U_r^{t+\tau} + (1-\theta) U_r^t]. \tag{36}$$

From (36) the amplification factor A is given by

$$A = |[1 - \lambda(1-\theta)\tau]/(1 + \lambda\theta\tau)| \tag{37}$$

where $\lambda = kQ\phi_r f_r^2(1)/h$.

In the case of the explicit scheme ($\theta = 0{\cdot}0$) this requires that

$$\tau \leqslant 2h/kQ\phi_r f_r^2(1). \tag{38}$$

For the boundary condition (18), typically $f_r^2 = 1$ and $\phi_r \approx 2$. For very shallow near-coastal regions a typical strong current is of the order $Q \approx 2\ \mathrm{m\,s^{-1}}$, $k = 0{\cdot}005\ \mathrm{m\,s^{-1}}$ and $h = 1$ m, giving τ of the order of 50 s or less, which in shallow near-coastal regions is prohibitive in terms of computer time. In theory, time centring or computing the frictional term at the higher time step would give an unconditionally stable scheme (e.g. equation (32)). However, as we will show later, this does not occur owing to the summation term in (35) which couples all the equations.

In order to obtain an unconditionally stable scheme, all the equations must be considered, giving

$$I\frac{d\mathbf{U}}{dt} = -\theta \mathbf{K}\mathbf{u}^{t+\tau} - (1-\theta)\mathbf{K}\mathbf{u}^t, \tag{39}$$

where $d\mathbf{U}/dt$ is a vector with rth element dU_r/dt, $\mathbf{I}$ is the unit matrix, $\mathbf{u}^{t+\tau}$ is a vector with rth element $u_r^{t+\tau}$ and $\mathbf{K}$ is a full matrix given by

$$\mathbf{K} = \begin{bmatrix} \frac{kQ}{h} f_1 \phi_1 f_1 & \frac{kQ}{h} f_1 \phi_2 f_2 & \cdots & \frac{kQ}{h} f_1 \phi_m f_m \\ \\ \frac{kQ}{h} f_m \phi_1 f_1 & \frac{kQ}{h} f_m \phi_2 f_2 & \cdots & \frac{kQ}{h} f_m \phi_m f_m \end{bmatrix}, \tag{40}$$

with $f_r = f_r(1)$.

Obviously time centring or evaluating the right-hand side of (39) at a higher time step would involve the formation of a matrix $\mathbf{K}$ at each grid point and a matrix solution which is clearly impractical.

An alternative approach is to update each U_i in equation (35) with its value at a higher time level, as it becomes available, and to centre this in time by performing essentially an upsweep and downsweep solution. Thus

upsweep, $r=1, 2, \ldots, m$

$$\frac{U_r^{t+\tau}-U_r^t}{\tau}=-\frac{kQ\phi_r f_r^2(1)}{h}[\theta U_r^{t+\tau}+(1-\theta)U_r^t]-\frac{kQ}{h}f_r(1)\left(\sum_{i=1}^{r-1}U_i^{t+\tau}\phi_i f_i(1)+\sum_{j=r+1}^{m}U_j^t\phi_j f_j(1)\right), \tag{41}$$

downsweep, $r=m, m-1, \ldots, 1$

$$\frac{U_r^{t+\tau}-U_r^t}{\tau}=-\frac{kQ\phi_r f_r^2(1)}{h}[\theta U_r^{t+\tau}+(1-\theta)U_r^t]-\frac{kQ}{h}f_r(1)\left(\sum_{i=1}^{r-1}U_i^t\phi_i f_i(1)+\sum_{j=r+1}^{m}U_j^{t+\tau}\phi_j f_j(1)\right), \tag{42}$$

with θ determining the time level of U_r and upsweep and downsweep applied at alternative time steps.

As will be shown later, this approach yields a computationally stable solution without matrix inversion. However, as will also be shown, with very large time steps in the case of low eddy viscosity some numerical damping can occur.

4. NUMERICAL CALCULATIONS

4.1. Wind-induced motion in the North Sea rectangle

Wind-induced flow in a North Sea rectangular basin has now become accepted as a 'benchmark' calculation for any new three-dimensional model development and has been used by a number of authors.[11,16,21–23] This problem is therefore ideal for comparing the various numerical methods for time discretization when the bottom boundary condition is treated as a natural boundary condition as compared with when it is satisfied exactly.

The closed rectangular North Sea basin ('the Heaps rectangle') has dimensions of 400 km in the x-direction and 800 km in the y-direction. A uniform staggered grid (Figure 2)[19] was used in the horizontal with grid spacing $\Delta x=400/9$ km and $\Delta y=800/17$ km, with water depth $h=65$ m, Coriolis parameter $\gamma=1{\cdot}2\times10^{-4}\,\mathrm{s}^{-1}$, with $\rho=1025\,\mathrm{kg\,m}^{-3}$ and $g=9{\cdot}81\,\mathrm{m\,s}^{-2}$.

In order to readily compare the calculations with the earlier ones of Heaps,[11] a linear slip condition was used, i.e. $Q=1$ in equation (10). By this means both the natural and essential boundary conditions could be compared (Table I). However, to test the relative stability conditions of the methods, a range of k-values was used, from $k=0{\cdot}002\,\mathrm{m\,s}^{-1}$ (originally used by Heaps[11]) up to an extremely high value of $k=0{\cdot}04\,\mathrm{m\,s}^{-1}$ (designed to test the numerical stability of the method). Also, a range of eddy viscosity values was used, from $\mu=0{\cdot}0650\,\mathrm{m}^2\,\mathrm{s}^{-1}$ (a value employed by Heaps[11]) down to a value of $0{\cdot}0065\,\mathrm{m}^2\,\mathrm{s}^{-1}$. In all cases the eddy viscosity was constant in the vertical. Motion in the rectangle was induced from a state of rest by a suddenly imposed wind stress of $F_S=0{\cdot}0$ and $G_S=-1{\cdot}5\,\mathrm{N\,m}^{-2}$. A time step of 360 s was used in the calculations.

Profiles of the first five modes, with μ constant at $130\,\mathrm{cm}^2\,\mathrm{s}^{-1}$ and k increasing from 0·002 to $0{\cdot}04\,\mathrm{m\,s}^{-1}$, computed initially subject to a zero-stress condition and then by satisfying boundary condition (20), are shown in Figure 1. It is clear from this figure that as k is increased, the modes, particularly the higher modes, show a marked reduction in the near-bed region with increasing shear in this layer.

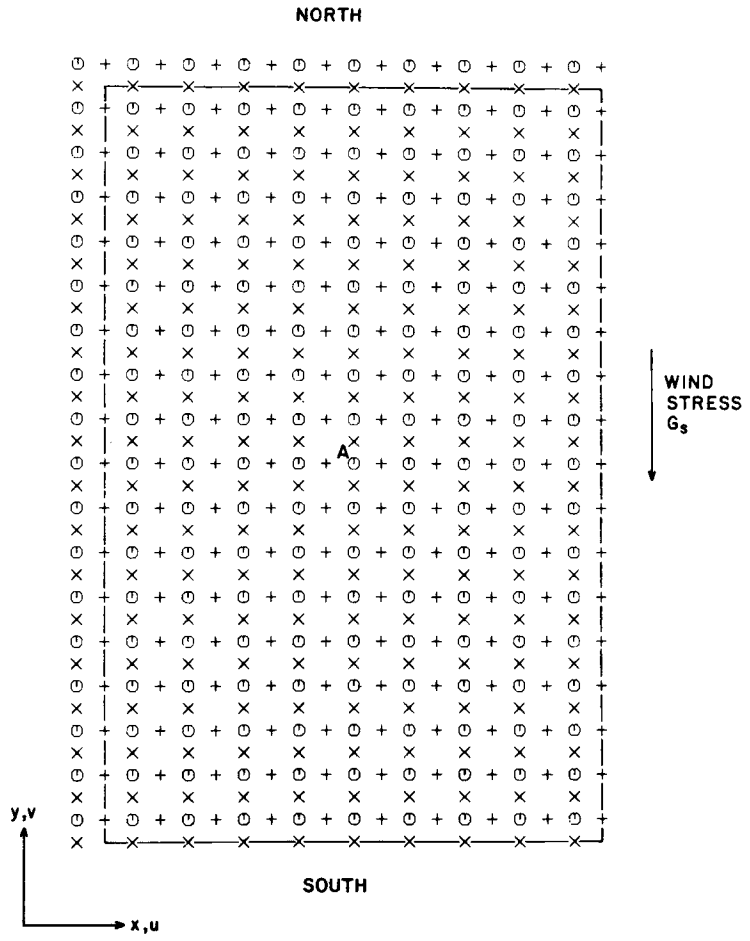

Figure 2. North Sea basin used in the calculation: ⊙, ζ-point; +, u-point, ×, v-point

Modes computed subject to the natural boundary condition (18) are of course independent of the value of k and have zero vertical derivative at the sea bed (Figure 1(a)). A consequence of this is that they are not highly sheared in the sea bed region. However, as we will show later, they do yield accurate current profiles and are the only satisfactory means of including a quadratic form of friction within the model. Recently, Davies *et al.*[18] have shown that modes of this form, where the first mode is the only one which contributes to the depth mean flow, are ideal for solution using time-splitting algorithms on multiprocessor vector computers.

It is evident from the analysis presented in Section 2 (equation (29)) that when the bottom boundary condition is satisfied exactly, the friction coefficient k does not appear in the hydrodynamic equations. However, its effect is included within the eigenvalue, the magnitude of which increases as k increases (see Table II).

In the case of the natural boundary condition the bottom friction term appears explicitly in the equations and increasing k has no influence on the eigenvalues. It is only the bottom stress term which damps the first mode.

Table I. Values of μ and k used in the various calculations and the stability of the solution depending upon the use of an essential (viscosity time-centred) or natural boundary condition. A time step of 360 s was used in the calculations

			Stable solution			
				Natural BC		
Calc.	μ ($m^2 s^{-1}$)	k ($m s^{-1}$)	Essential BC Viscosity at $\theta = 0{\cdot}5$	Bottom friction at $\theta = 1$ or 0·5	Viscosity at $\theta = 1$ or 0·5	Time sweep
A	0·0650	0·002	Yes	Yes	Yes	Yes
B	0·0650	0·02	Yes	No	No	Yes
C	0·0130	0·002	Yes	Yes	Yes	Yes
D	0·0130	0·02	Yes	No	No	Yes
E	0·0130	0·04	Yes	No	No	Yes
F	0·0065	0·02	Yes	No	No	Yes
G	0·0065	0·04	Yes	No	No	Yes

Table II. The first five eigenvalues normalized with respect to the eddy viscosity, computed with $\mu = 0{\cdot}0130\ m^2 s^{-1}$, for a range of k-values

Mode number	Essential BC			
r	$k = 0{\cdot}002\ m s^{-1}$	$k = 0{\cdot}02\ m s^{-1}$	$k = 0{\cdot}04\ m s^{-1}$	Natural BC
1	2·0420	2·4180	2·4430	0·0
2	18·542	21·772	21·987	9·870
3	52·244	60·466	61·074	39·478
4	104·04	118·527	119·706	88·826
5	174·610	195·944	197·880	157·914

It is clear from Table III and the previous analyses that by centring the viscosity term in time, an unconditionally stable scheme is obtained for all values of μ and k used in the calculation when the bottom boundary condition is treated as an essential boundary. However, in the case of the bottom boundary condition treated as a natural boundary condition, time centring or evaluating the viscosity and frictional terms at the higher time step did not lead to increased stability when the bottom friction coefficient was increased above $0{\cdot}002\ m s^{-1}$ with a time step of 360 s, and wind-induced currents in the rectangular basin quickly became unstable. However, by using the time sweep approach, a stable algorithm could be obtained with a time step of 360 s and high k-values, giving a physically realistic wind-induced flow field in the basin, in good agreement with that found using an essential boundary condition (Table III).

To check that the time sweep algorithm had not achieved stability by excessive damping of the solution, current profiles at the centre of the basin, computed using 10 modes, 30 h after the onset of the wind field were determined (Table III). It is evident from this table and from plots of current profiles (Figure 3) that there were no major differences between currents computed satisfying the bottom boundary condition exactly and those determined using a natural boundary condition with the sweep method of solution. Current values and profiles computed with the sweep method

Table III. Surface and bed currents (cm s^{-1}) at the centre of the North Sea rectangle (point A in Figure 2) 30 h after the imposition of the wind field, computed (1) satisfying the bottom boundry condition exactly and (2) using a natural boundary condition with the time sweep algorithm. Ranges of μ- and k-values were used in the calculations (see Table I)

		Calculation						
		$\mu = 650$ cm^2 s^{-1} $k = 0{\cdot}002$ m s^{-1} A	$\mu = 650$ cm^2 s^{-1} $k = 0{\cdot}02$ m s^{-1} B	$\mu = 130$ cm^2 s^{-1} $k = 0{\cdot}002$ m s^{-1} C	$\mu = 130$ cm^2 s^{-1} $k = 0{\cdot}02$ m s^{-1} D	$\mu = 130$ cm^2 s^{-1} $k = 0{\cdot}04$ m s^{-1} E	$\mu = 65$ cm^2 s^{-1} $k = 0{\cdot}02$ m s^{-1} F	$\mu = 65$ cm^2 s^{-1} $k = 0{\cdot}04$ m s^{-1} G
Essential BC								
Surface	U_S	− 15·07	− 10·55	− 66·71	− 66·26	− 66·22	− 98·61	− 98·66
	V_S	− 32·14	− 34·62	− 65·41	− 70·60	− 71·10	− 85·88	− 86·14
Bed	U_B	7·12	1·32	9·06	1·28	0·65	0·70	0·35
	V_B	11·09	2·53	4·95	0·98	0·50	0·72	0·36
Natural BC								
Surface	U_S	− 14·83	− 9·99	− 66·34	− 65·64	− 65·56	− 98·54	− 98·63
	V_S	− 32·18	− 34·52	− 65·89	− 71·75	− 72·31	− 85·77	− 86·11
Bed	U_B	7·40	1·35	9·77	1·37	0·69	0·69	0·35
	V_B	11·41	2·63	5·39	1·16	0·61	0·95	0·48

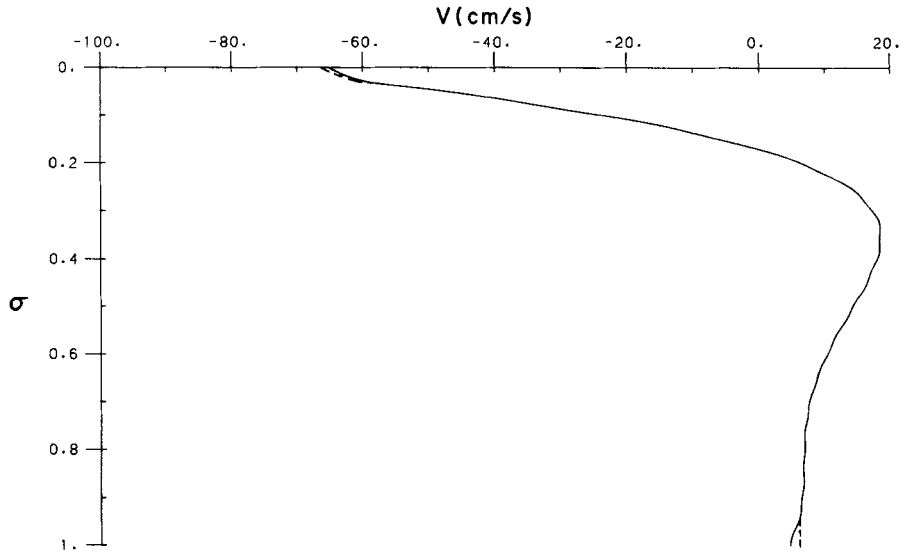

Figure 3. Profile of v-current at point A in the centre of the basin 30 h after the onset of the wind field, computed with $\mu = 0{\cdot}0130\ m^2\,s^{-1}$ and $k = 0{\cdot}002\ m\,s^{-1}$, with an essential boundary condition (——) and a natural boundary condition (– – – –)

were also in excellent agreement with published values determined by other methods, e.g. grid box, Legendre or Chebyshev polynomials.[16]

4.2. *Oscillatory flow*

In the previous series of calculations, current profiles were induced by wind forcing. It is clear from equations (27) and (28) that in the case of wind-forced motion and a natural bottom boundary condition each mode is excited by the wind stress and damped by the bottom friction and eddy viscosity (excluding the first mode, which is only damped by the bottom friction).[20]

Although it is instructive to compare current profiles for the North Sea rectangle generated by this means, a more rigorous test of the model is to compare the performance of the sweep method with other methods when motion is generated by an oscillatory pressure forcing alone. It is apparent from equations (27) and (28) that in the absence of an external wind stress an oscillatory pressure gradient only drives the first mode directly, with the higher modes which produce the current structure being forced by the bed stress—a problem that provides a more rigorous test of the sweep method of solution.

As in the previous series of calculations, ranges of eddy viscosity values and bottom friction coefficients were used, but in this case the water depth was set at a low value, initially 5 m, so that frictional effects would reach the surface. Also, a range of time steps was used in order to determine how much inaccuracy was introduced by using a 'long' time step. An expansion of 10 modes in the vertical was used in all calculations.

Eddy viscosity $\mu = 0{\cdot}0130\ m^2\,s^{-1}$. Initial calculations ($\mu = 0{\cdot}0130\ m^2\,s^{-1}$, $k = 0{\cdot}002\ m\,s^{-1}$) with a time step of 180 s showed little difference between the amplitude and phase of the surface and bottom currents computed using both the original method and the sweep method, with both remaining stable (Table IV). However, when the bottom friction coefficient was increased to

Table IV. Influence of evaluating friction and viscosity at various time levels with and without the sweep method upon current amplitude and phase in a water depth $h = 5$ m with $\mu = 130\ \mathrm{cm^2\,s^{-1}}$

					Analysis			
					Surface		Bed	
k (m s^{-1})	τ (s)	θ (fric)	θ (visc)	Sweep	h_u (cm s^{-1})	g_u (deg)	h_u (cm s^{-1})	g_u (deg)
0·002	180	1·0	1·0	No	45·5	203·4	33·3	202·8
	180	1·0	1·0	Yes	45·1	204·7	32·9	203·7
0·02	18	0·0	0·5	No	16·8	188·7	3·6	187·4
	45	0·5	0.5	No		Unstable 54τ		
	45	1·0	1·0	No		Unstable 84τ		
	180	1·0	1·0	Yes	16·7	190·7	3·6	190·5
	360	1·0	1·0	Yes	16·5	193·3	3·5	194·0
0·03	18	0·0	0·0	No	15·6	188·4	2·4	187·1
	45	1·0	0·0	No		Unstable 25τ		
	180	1·0	1·0	Yes	15·5	191·4	2·4	191·6
	360	1·0	1·0	Yes	15·2	195·1	2·3	196·7
0·05	180	1·0	1·0	No		Unstable 80τ		
	360	1·0	1·0	No		Unstable 68τ		
	180	1·0	1·0	Yes	14·4	193·3	1·4	194·6
	360	1·0	1·0	Yes	13·9	199·2	1·4	202·9

0·02 m s^{-1}, the non-sweep method only remained stable with a time step of 18 s even if the viscosity and friction term for the rth mode (equation (36)) were evaluated at the higher time step. Applying the sweep method (equations (41) and (42)), however, yielded a stable solution. With a time step of the order 360 s the surface current, although damped, was determined to an acceptable level of accuracy (compared to the 18 s time step).

Increasing the bottom friction to 0·03 m s^{-1}, a stable solution could still be obtained with the non-sweep method with a time step of 18 s, although with an increased value (45 s) the solution was unstable after 25 time steps. However, the sweep method remained stable and accurate (Table IV). With the bottom friction at 0·05 m s^{-1} the non-sweep method with a time step of 18 s was also unstable. Only the sweep method appeared stable with such high friction coefficients.

Eddy viscosity $\mu = 0{\cdot}1300\ m^2\,s^{-1}$. In a second series of calculations, to examine the influence of the eddy viscosity upon the stability of the solution, μ was increased to 0·1300 m^2 s^{-1}. From the stability analysis presented earlier (equation (33) for five modes, $\varepsilon_5 \approx 160$), if the viscosity term was evaluated at the lower time step then the time step would have to be below 2 s, which was borne out by calculation. However, with the bottom friction and viscosity terms evaluated at the higher time step, both the non-sweep and sweep methods remained stable, with no significant difference between the computed solutions (see Table V). Ten modes were used in these calculations. This suggests that when the viscosity term is large and evaluated at the higher time step, the modal damping introduced is sufficient to stabilize any instability due to bottom friction. Also, with such high viscosity any numerical damping is negligible compared with the physical damping. To test this, a series of calculations was performed with μ reduced to 0·0013 m^2 s^{-1}.

Eddy viscosity $\mu = 0{\cdot}0013\ m^2\,s^{-1}$. With $\mu = 0{\cdot}0013$ m^2 s^{-1} and $k = 0{\cdot}02$ m s^{-1} the non-sweep method using 10 modes in the vertical was only stable with a time step of the order of 18 s (see Table VI). The sweep method did, however, remain stable, although as the length of the time step

Table V. As Table IV but with $\mu = 1300\ cm^2\ s^{-1}$

					Analysis			
					Surface		Bed	
k ($m\ s^{-1}$)	τ (s)	θ (fric)	θ (visc)	Sweep	Amplitude ($cm\ s^{-1}$)	Phase (deg)	Amplitude ($cm\ s^{-1}$)	Phase (deg)
0·02	18	1·0	1·0	No	4·96	182·7	3·62	182·7
	180	1·0	1·0	Yes	4·96	182·9	3·62	182·9
	360	1·0	1·0	Yes	4·96	183·3	3·63	183·3
0·03	180	1·0	1·0	Yes	3·76	182·4	2·42	182·4
	360	1·0	1·0	Yes	3·75	182·9	2·42	183·0
0·05	180	1·0	1·0	Yes	2·81	182·2	1·45	182·2
	360	1·0	1·0	Yes	2·81	182·9	1·45	183·1

Table VI. As Table IV but with $\mu = 0{\cdot}0013\ m^2\ s^{-1}$

					Analysis			
					Surface		Bed	
k ($m\ s^{-1}$)	τ (s)	θ (fric)	θ (visc)	Sweep	Amplitude ($cm\ s^{-1}$)	Phase (deg)	Amplitude ($cm\ s^{-1}$)	Phase (deg)
0·02	18	0·5	0·5	No	89·5	231·0	2·50	217·0
	18	1·0	0·5	No	87·3	232·2	2·40	217·3
	45	1·0	1·0	Yes	86·4	232·1	2·36	221·6
	90	1·0	1·0	Yes	81·6	234·1	2·21	226·3
	180	1·0	1·0	Yes	73·3	237·5	1·97	235·1
	360	1·0	1·0	Yes	60·5	242·7	1·58	250·9
0·03	180	1·0	1·0	No		Unstable 26τ		
	180	1·0	1·0	Yes	66·6	240·5	1·31	243·2
	360	1·0	1·0	Yes	51·3	247·1	0·96	265·0
0·05	180	1·0	1·0	No		Unstable 22τ		
	180	1·0	1·0	Yes	55·6	245·5	0·58	259·0
	360	1·0	1·0	Yes	38·7	253·4	0·41	292·5

was increased, the magnitude of the amplitude of the surface current was reduced, indicating significant numerical damping (Table VI). With increasing bottom friction the sweep method remained stable, although it is evident from Table VI that increasing the time step from 180 to 360 s introduces numerical damping.

Although this test problem is numerically very interesting, it is probably not physically very realistic in that in shallow water, strong currents flowing over a rough bed (a high-friction regime) would generate significant turbulence in the water column (a high eddy viscosity value).

Eddy viscosity $\mu = 0{\cdot}0130\ m^2\ s^{-1}$, water depth $h = 1\ m$. In a final series of calculations the water depth h was reduced to 1 m, the minimum water depth that it is reasonable to resolve in a numerical model before drying occurs. It is evident from Table VII that in such a region the non-sweep method even with $\tau = 18$ s becomes unstable after about 100 time steps. Solutions with the

Table VII. As Table IV but in a water depth $h = 1$ m with $\mu = 0{\cdot}0130\ m^2\ s^{-1}$

					Analysis			
					Surface		Bed	
k ($m\ s^{-1}$)	τ (s)	θ (fric)	θ (visc)	Sweep	Amplitude ($cm\ s^{-1}$)	Phase (deg)	Amplitude ($cm\ s^{-1}$)	Phase (deg)
0·02	18	1·0	0·5	No		Unstable 104τ		
	18	0·5	0·5	No		Unstable 77τ		
	180	1·0	1·0	Yes	1·26	181·3	0·73	181·4
	360	1·0	1·0	Yes	1·26	181·9	0·73	182·0
0·03	180	1·0	1·0	Yes	1·02	181·4	0·49	181·6
	360	1·0	1·0	Yes	1·02	182·3	0·48	182·6
0·05	180	1·0	1·0	Yes	0·83	181·8	0·29	182·1
	360	1·0	1·0	Yes	0·83	183·3	0·29	184·0

sweep method, however, remained stable, although owing to the high bed damping the currents were very small.

Although the problem is of some interest from the numerical point of view, physically the currents are so low that it would be impossible to measure them with any degree of accuracy.

It is apparent from this series of calculations that when the frictional coefficient is low, the non-sweep method remains stable with time steps of the order of 180 s. However, with increased friction coefficient and reduced eddy viscosity a time step of the order of 18 s was required to maintain stability with the non-sweep method, although the sweep method remained stable.

5. CONCLUDING REMARKS

It is evident from the mathematical analysis presented in this paper that when the hydrodynamic equations are solved using a set of modes satisfying a slip bottom boundary condition, a stable time-stepping algorithm can be readily developed by centring the viscosity term in time or evaluating it at the higher time level. Such a method is, however, restricted to a linear form of bottom friction. Also, in a 'real world model' incorporating variations in bottom topography the value of kh/μ must be constant[20] unless a different basis set of functions is to be used at each grid point with an associated high computational cost.

Physically a quadratic form of bottom friction is more appropriate. However, in this case the bottom friction has to be included as a natural boundary condition. It is evident from the analysis presented here and the numerical calculations that evaluating the viscosity term centred in time or at the higher time level does not yield a stable solution when the bottom friction is high, the eddy viscosity is low and the water depth is shallow. However, the new numerical algorithm developed here, in which the modal contribution to the bed stress is updated as modal coefficients at the higher time level are computed, in a 'sweep form' does appear to yield a stable numerical solution at significantly longer time steps (of the order of 360 s compared wth 18 s) than with a non-sweep solution.

A comparison of computed currents using the sweep method with $\tau = 360$ s and the non-sweep method with $\tau = 18$ s clearly demonstrated the accuracy and stability of the approach. However, for low eddy viscosity values the sweep method with a long time step does introduce some numerical damping. Although the case of low eddy viscosity is numerically interesting, it is not

physically very realistic. Consequently, provided a time step of the order of 180–360 s is used in a 'real world model', a stable accurate solution should be obtained using the sweep method developed in this paper.

The modal method developed here has recently been combined with a turbulence energy approach. Calculations[24] have demonstrated that the modal method is as accurate as a turbulence energy approach at a fraction of the computational cost. Also, modal methods can generate the higher tidal harmonics and with the addition of functions to represent highly sheared surface layers[25] can accurately reproduce the surface currents.

The sweep algorithm developed in this paper has proved to be particularly stable in a three-dimensional model of flow in a near-coastal shallow region of the Irish Sea, including a drying condition. The model is presently being used to examine the physical oceanography of this region and results will be reported subsequently.

ACKNOWLEDGEMENTS

The authors are indebted to R. A. Smith for preparing the diagrams and to J. Hardcastle for typing this paper.

One of us (J. N. A.) would like to express his thanks to the Director of POL for computing facilities, etc. during his stay and to MAFF for a year's leave of absence.

REFERENCES

1. M. L. Spaulding and T. Isaji, 'Three dimensional continental shelf hydrodynamic model including wave current interaction', in J. C. J. Nihoul and B. M. Jamart (eds), *Three-dimensional Models of Marine and Estuarine Dynamics*, Elsevier, Amsterdam, 1987, pp. 405–426.
2. A. M. Davies, 'Application of the Dufort–Frankel and Saul'ev methods with time splitting to the formulation of a three dimensional hydrodynamic sea model', *Int. j. numer. methods fluids*, **5**, 405–425 (1985).
3. I. D. James, 'Numerical modelling of density-driven circulation in shelf seas', in A. M. Davies (ed.), *Modeling Marine Systems. Vol. 2*, CRC Press, Florida, 1991.
4. J. Noye and M. Stevens, 'A three-dimensional model of tidal propagation using transformations and variable grids', in N. S. Heaps (ed.), *Three-dimensional Coastal Ocean Models*, AGU, Washington, 1987, pp. 41–70.
5. A. M. Davies, 'On the accuracy of finite difference and spectral methods for computing tidal and wind wave current profiles', *Int. j. numer. methods fluids*, **12**, 101–124 (1991).
6. J. J. Leendertse, R. C. Alexander and S. K. Liu, 'A three-dimensional model for estuaries and coastal seas. Vol. 1: Principles of computation', *Report R-1417-OWER*, Rand Corp., Santa Monica, CA, 1973.
7. M. B. Abbott, 'Numerical modeling for coastal and ocean engineering', in J. B. Herbich (ed.), *Handbook of Coastal and Ocean Engineering, Vol. 2: Offshore Structures, Marine Foundations, Sediment Processes and Modeling*, Gulf Publishing, Houston, TX, 1991, pp. 1067–1124.
8. D. R. Lynch and C. B. Officer, 'Analytic test cases for three-dimensional hydrodynamic models', *Int. j. numer. methods fluids*, **5**, 529–543 (1985).
9. D. R. Lynch and F. E. Werner, 'Three-dimensional hydrodynamics on finite elements. Part 1: Linearised harmonic model', *Int. j. numer. methods fluids*, **7**, 871–909 (1987).
10. F. E. Werner, 'A numerical study of secondary flows over continental shelf edges', *Continental Shelf Res.*, **7**, 379–409 (1987).
11. N. S. Heaps, 'On the numerical solution of the three dimensional hydrodynamical equations for tides and storm surges', *Mem. Soc. Sci. Liege Ser. 6*, **2**, 143–180 (1972).
12. O. C. Zienkiewicz and J. C. Heinrich, 'A unified treatment of steady-state shallow water and two-dimensional Navier–Stokes equations—finite element penalty function approach', *Comput. Methods Appl. Mech. Eng.*, **17/18**, 673–698 (1979).
13. R. B. Gordon and M. L. Spaulding, 'Numerical simulations of the tidal- and wind-driven circulation in Narragansett Bay', *Estuar., Coastal Shelf Sci.*, **24**, 611–636 (1987).
14. G. K. Furnes, 'A three dimensional numerical sea model with eddy viscosity varying piecewise linearly in the vertical', *Continental Shelf Res.*, **2**, 231–242 (1983).
15. G. K. Furnes and M. Mork, 'Formulation of a continuously stratified sea model with three-dimensional representation of the upper layer', *Coastal Eng.*, **11**, 415–445 (1987).
16. A. M. Davies and C. V. Stephens, 'Comparison of the finite difference and Galerkin methods as applied to the solution of the hydrodynamic equations', *Appl. Math. Model.*, **7**, 226–240 (1983).

17. A. M. Davies and R. Proctor, 'Developing and optimizing a 3D-spectral/finite difference hydrodynamic model for the CRAY X-MP', *Comput. Fluids*, **18**, 259–270 (1989).
18. A. M. Davies, R. B. Grzonka and C. V. Stephens, 'Implementation of a three dimensional hydrodynamic numerical model using parallel processing on a CRAY X-MP series computer', *Adv. Parallel Comput.*, in the press.
19. A. M. Davies, 'Formulation of a linear three-dimensional hydrodynamic sea model using a Galerkin–eigenfunction method', *Int. j. numer. methods fluids*, **3**, 33–60 (1983).
20. A. M. Davies, 'Spectral models in continental shelf sea oceanography', in N. S. Heaps (ed.), *Three-dimensional Coastal Ocean Models*, AGU, Washington, 1987, pp. 71–106.
21. A. M. Davies and A. Owen, 'Three-dimensional numerical sea model using the Galerkin method with a polynomial basis set', *Appl. Math. Model.*, **3**, 421–428 (1979).
22. B. M. Jamart and J. Ozer, 'Numerical boundary layers and spurious residual flows', *J. Geophys. Res.*, **91**, 10621–10631 (1986).
23. R. W. Lardner and H. M. Cekirge, 'A new algorithm for three-dimensional tidal and storm surge computations', *Appl. Math. Model.*, **12**, 471–481 (1988).
24. A. M. Davies, 'On using turbulence energy models to develop spectral viscosity models', *Continental Shelf Res.*, in the press.
25. A. M. Davies, 'Solution of the 3D linear hydrodynamic equations using an enhanced eigenfunction approach', *Int. j. numer. methods fluids* **13**, 235–250 (1991).